# Size-dependent structural transition from multiple-twinned particles to epitaxial fcc nanocrystals and nanocrystal decay

K. Sato,* W. J. Huang, F. Bohra, S. Sivaramakrishnan, A. P. Tedjasaputra, and J. M. Zuo
*Department of Materials Science and Engineering and Frederick Seitz Materials Research Laboratory, University of Illinois at Urbana-Champaign, Urbana, Illinois 61801, USA*
(Received 8 June 2007; revised manuscript received 8 September 2007; published 26 October 2007)

The size dependence of structural transition from multiple-twinned particles (MTP) to epitaxial face centered cubic nanocrystals was investigated for Ag nanoparticles formed on Si(001) surfaces by *in situ* reflection high-energy electron diffraction and *ex situ* transmission electron microscopy. The transition from MTP to nanocrystals was promoted by postdeposition annealing. Clear particle size dependence is found in the epitaxial formation temperatures ($T_E$), which is about 2/3 of the calculated, size-dependent, melting temperature ($T_M$) using the value of surface energy $\gamma_S$=1.2 J/m$^2$ for larger particles (>2 nm). Once nanocrystals are formed, they decay and disappear in a narrow temperature range between 795 and 850 K. No evidence of nanocrystal melting was detected from the reflection high-energy electron diffraction observations.

DOI: 10.1103/PhysRevB.76.144113 PACS number(s): 61.46.Df, 64.70.Nd, 61.14.Hg, 68.37.Lp

## I. INTRODUCTION

Recent interest in metallic nanoparticles have drawn renewed attention to a class of multiple-twinned particles (MTP) that are characterized by the preference of {111} facets, presence of the five-fold symmetry, and elastic deformation of the constituent tetrahedral domains. The MTPs were first observed in small gold particles forty years ago.[1] Subsequent studies have shown that MTPs are stabilized by the competition between the elastic strain and the favorable surface energies and there is a critical size beyond which the bulk crystal structure is preferred.[2] In the case of Ag, molecular dynamics (MD) simulations predict that particles larger than 8 nm are expected to adopt the bulk, face centered cubic (fcc), structure.[3] MD simulations also show that the differences in the energies of different structural forms are small. Experimentally, once MTPs are formed, significant atomic rearrangements are required to transform to the fcc structure. The transformation from MTPs to fcc has been rarely studied. It can be assumed that as the particle continues to grow, the transformation becomes increasingly difficult for larger particles. Experimentally, it has been shown that in an inert-gas-aggregation source the MTPs can attain considerable sizes.[4] It has also been suggested that structure transformation in large particles would require complete particle melting[4,5] or grain growth.[6] The melting of nanoparticles is size-dependent.[7–9] In case of Ag nanoparticles, lowering of the melting temperature has been clearly shown by Castro *et al.*[10] and Shyjumon *et al.*[11] as a function of the particle size. The depression of the melting temperature can be explained by the thermodynamical model[7,12] based on the Gibbs-Thomson effect, which predicts a continuous decrease of the melting temperature when the particle size reduces.[10–13] Similar size dependence is expected for the MTP to fcc transition if nanoparticle melting is involved.

Previously, one of the authors has shown that most of the Ag nanoparticles formed on hydrogen terminated Si(001) (H-Si(001)) are MTPs and they transformed to epitaxial fcc nanocrystals upon annealing.[14] The driving force for the transition comes from the strain energy of the Ag MTPs and a possible change in interfacial energy at the Ag-Si interface.[14] The driving force appears large enough that even MTPs with diameters as small as 2 nm transform into fcc nanocrystals. Thus Ag nanoparticles on H-Si(001) are ideal for studying the size dependence of transformation from MTP to fcc. Here we report an *in situ* reflection high-energy electron diffraction (RHEED) observation of nanoparticle structure transformation during the postdeposition annealing. *Ex situ* TEM is carried out to characterize the morphology and size distribution of Ag nanoparticles grown on H-Si(001) substrate. The experiment was carried out as a function of particle size. Furthermore, using the same experimental setup, we investigated the size dependence of the decay of epitaxial Ag nanocrystals. The experimental results are discussed in the context of recent articles on structural and thermodynamical properties of small metal nanoparticles.

## II. EXPERIMENT

Ag nanoparticles were prepared by electron-beam deposition of high-purity Ag (99.9999%) onto chemically prepared H-Si(001) substrates ($6\times15\times0.5$ mm$^3$) at room temperature. The deposition and subsequent annealing were carried out in a vacuum chamber equipped with a RHEED gun (base pressure of $\sim10^{-7}$ Pa). The growth rate was monitored using a quartz oscillator and calibrated by *ex situ* Rutherford backscattering spectroscopy. The growth rate was set at 0.1 nm/min. For *ex situ* TEM observation, the Si(001) substrates were initially back-thinned by grinding, followed by the chemical etching for electron transparency. After degreasing and chemical cleaning, the samples were etched in a 40% $NH_4F$ solution, followed by a short rinse in deionized water, for hydrogen termination.[14] The surfaces of H-Si(001) substrates before and after the Ag deposition were characterized by RHEED operated at 11 kV (wavelength $\lambda$ =0.0116 nm). The diffraction patterns were recorded from areas unaffected by the thinning using a charge coupled device (CCD) camera. A tungsten-rhenium thermocouple attached to the sample heater was used to monitor the sample temperature. The temperature at the sample position was

 

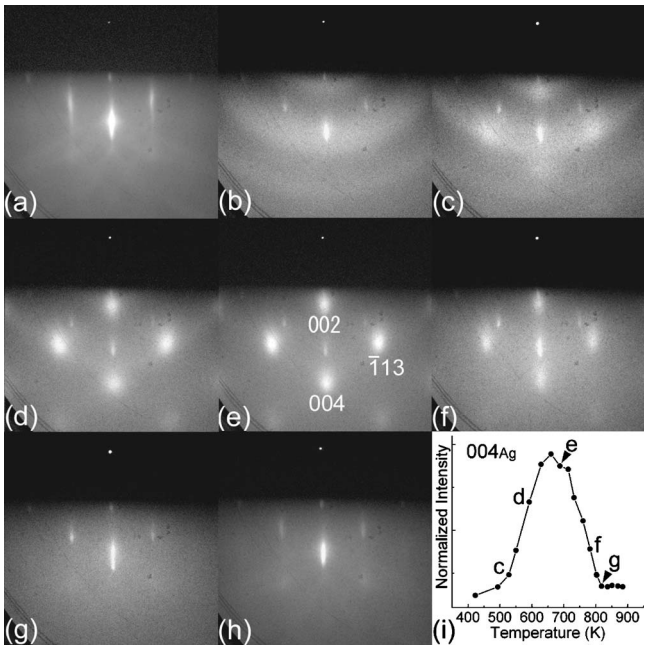


FIG. 1. RHEED patterns recorded *in situ* from Ag nanoparticles supported on H-Si(001) during the postdeposition annealing. The Ag coverage is 1.6 ML. The beam incidence is parallel to $[110]_{Si}$. (a) H-Si(001) before Ag deposition, (b) as-deposited, (c) 528 K, (d) 592 K, (e) 688 K, (f) 782 K, (g) 818 K, (h) after cooling down to the room temperature, and (i) change in $(004)_{Ag}$ reflection intensity during the *in situ* annealing. The development of Ag epitaxy followed by Ag disappearance on the H-Si(001) substrate are clearly seen during the course of annealing. The orientation relationship between Ag and Si is as follows: $(001)_{Ag}\|(001)_{Si}$, $[110]_{Ag}\|[110]_{Si}$.

calibrated prior to the *in situ* annealing of Ag nanoparticles using a chromel-alumel thermocouple. The heating rate was set to be about 5 K/min. Particle morphology and selected area electron diffraction (SAED) patterns were observed *ex situ* by using a JEOL 2010F TEM operated at 200 kV with a field emission gun. All TEM images were recorded by a CCD camera, while SAED patterns were recorded by using Imaging Plates (Fuji Film FDL-UR-V). Elemental analyses of the samples before and after annealing were carried out by using an energy dispersive x-ray spectrometer (EDS, Oxford INCA) attached to the TEM, and also by x-ray photoelectron spectroscopy (XPS, Kratos Axis ULTRA) using a monochromatic Al $K_\alpha$ source and a charge neutralizer.

## III. RESULTS AND DISCUSSION

Figure 1 shows a series of RHEED patterns recorded during the course of Ag deposition and the subsequent annealing at high temperatures for the Ag coverage of 1.6 ML (monolayer). Before the Ag deposition, the H-Si(001) gave clear sharp diffraction streaks in the RHEED pattern indicating a smooth substrate surface [Fig. 1(a)]. The diffraction patterns were recorded using the beam incidence along $[110]_{Si}$. The incident angle of electrons was 2.1°, which was estimated from the position of the shadow edge, the specular spot, and the direct beam. After depositing a small amount of Ag at room temperature, broad Debye-Scherrer rings of Ag appear in the RHEED pattern [Fig. 1(b)], while weak diffraction streaks of H-Si(001) still remain. The diffraction pattern is consistent with the low coverage and Volmer-Weber growth of Ag. The ring diffraction pattern of Ag comes from the growth of Ag MTPs of random orientation on the H-Si(001), which was observed by TEM.[14] Lower surface energy of the H-terminated Si is responsible for the particle growth of Ag.[15] The TEM study shows that annealing of as-deposited Ag nanoparticles lead to a structural change from MTPs to fcc epitaxial nanocrystals.[14] The starting of transformation was observed in RHEED by the appearance of weak, broad diffraction peaks on the Ag diffraction rings at around 493 K. The Ag diffraction peaks grow stronger while the diffraction rings become weaker as the annealing temperature increases; this is clearly seen in Figs. 1(c) (528 K), 1(d) (592 K), and 1(e) (688 K). The spotlike Ag diffraction pattern comes from the 3D epitaxial Ag islands formed by annealing. The average Ag nanoparticle size is 2.4 nm, which was measured *ex situ* using TEM after the sample was annealed at 680 K. The Ag diffraction pattern belongs to the [110] zone axis. Note that the $(\bar{1}11)$ and $(1\bar{1}1)$ reflections of Ag are not visible in the RHEED pattern since these reflections are shadowed by the specimen. The orientation relationship between Ag and Si is $(001)_{Ag}\|(001)_{Si}$, $[110]_{Ag}\|[110]_{Si}$, in agreement with the previous paper.[14] Further annealing at 732 K led to the loss of Ag diffraction intensities. The change in $(004)_{Ag}$ intensity during *in situ* annealing is shown in Fig. 1(i) as a function of temperature. Figure 1(f) was taken at 782 K showing an apparent decrease in the Ag diffraction intensity. This was followed by a disappearance of Ag diffraction peaks at higher temperatures. After cooling down to the room temperature from the maximum annealing temperature of 888 K, only the streak pattern of Si(001) ([110] azimuth) is clearly seen [Fig. 1(h)]. Disappearance of the Ag reflections indicates Ag evaporation from Si(001) surface after melting or sublimation of Ag.[16,17] The difference between melting and sublimation will be further discussed later.

Following the same procedure, we examined the epitaxial transformation and nanocrystal decay behavior for a specimen with a Ag coverage of 3.2 ML. A series of *in situ* RHEED patterns are shown in Fig. 2 with a beam incident angle of 2.0°. The development of epitaxy and disappearance of Ag in the course of annealing are similar to those observed in the 1.6 ML Ag coverage shown in Fig. 1. There are also several differences observed by RHEED as follows. (1) No Si reflections, nor the specular spot, were observed due to the thicker Ag coverage. (2) An additional diffraction ring was observed in the as-deposited specimen indicated by the arrow in Fig. 2(b). The extra ring was indexed as the $(202)_{Ag}$ reflection with $[\bar{1}11]$ azimuth [Fig. 2(e)]. (3) The epitaxy of Ag started at 549 K, which is about 56 K higher than that for the 1.6 ML Ag coverage. (4) Weak Ag diffraction rings remained in the RHEED pattern after annealing up to 760 K [Fig. 2(e)], while the Ag reflections started to lose intensity after annealing at 796 K. (5) The loss of Ag diffraction intensity is accompanied by elongation of the diffraction peak in the direction normal to the substrate surface [Fig. 2(f)].

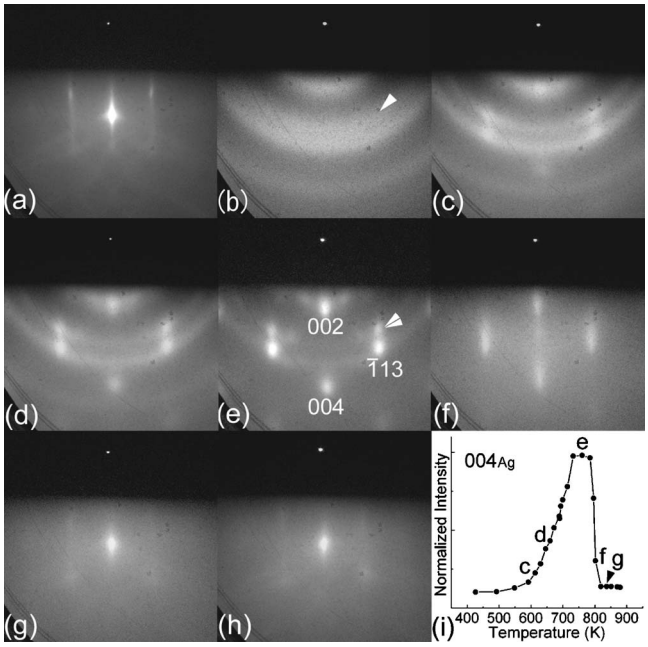


FIG. 2. RHEED patterns recorded *in situ* from Ag nanoparticles supported on H-Si(001) during the postdeposition annealing. The Ag coverage is 3.2 ML. The beam incidence is parallel to $[110]_{Si}$. (a) H-Si(001) before Ag deposition, (b) as-deposited, (c) 613 K, (d) 660 K, (e) 760 K, (f) 802 K, (g) 837 K, (h) after cooling down to the room temperature, and (i) change in $(004)_{Ag}$ reflection intensity during the *in situ* annealing. Reflection spot denoted by a double arrowhead in Fig. 1(e) comes from the Ag nanocrystals with beam incidence of along $[\bar{1}11]_{Ag}$. See text for details.

These two effects are clearly seen in the pattern taken at 782 K [Fig. 2(f)]. After the disappearance of the Ag reflections, Si reflections again appeared as shown in Fig. 2(g) (837 K). The change in $(004)_{Ag}$ intensity during *in situ* annealing is shown in Fig. 2(i). Figure 2(h) shows the RHEED pattern recorded after the sample cooled down to room temperature from the maximum annealing temperature of 880 K. The Si streaks after annealing are not as sharp as the original ones. A careful analysis of the RHEED pattern shows very weak $SiO_2$ diffraction intensity rings. The presence of $SiO_2$ was also supported by *ex situ* XPS analysis. The oxidation occurred at temperatures corresponding to hydrogen desorption, which are higher than the epitaxy formation temperature.[18,19] Hydrogen desorption also provides a part of the driving force for the Ag nanoparticle transition from MTPs to fcc nanocrystals.[14] No evidence of Ag oxidation was observed by RHEED. The additional weak $(202)_{Ag}$ reflections in Fig. 2(e) (shown by double-arrow head) comes from the Ag nanoparticles with a different orientation with $(1\bar{1}2)_{Ag}\|(001)_{Si}$, $[\bar{1}11]_{Ag}\|[110]_{Si}$.

Figure 3 compares the RHEED patterns obtained after the development of epitaxial Ag nanocrystals for a different Ag coverage. The four RHEED patterns were recorded at different temperatures since the annealing temperature required for transforming MTPs to nanocrystals increases with the Ag coverage. In each case, we also measured the nanocrystal size using TEM. The results are listed below for the amount

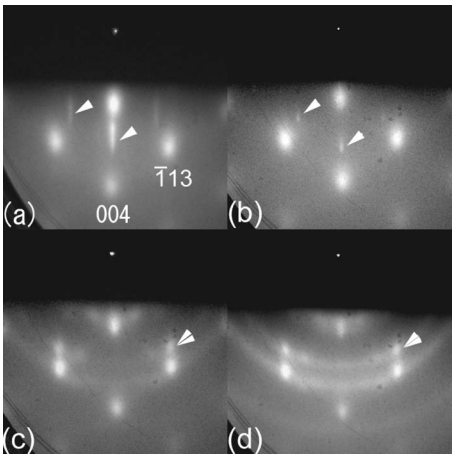


FIG. 3. The formation of epitaxial Ag nanocrystals with different Ag coverages. (a) 0.6 ML, observed at 670 K, (b) 1.6 ML at 688 K, (c) 3.2 ML at 760 K, and (d) 4.8 ML at 782 K. As the thickness increases, Si streaks (single arrow heads) disappear from the RHEED pattern and additional Ag reflections (double arrow heads) with $[\bar{1}11]$ azimuth as well as weak Debye-Scherrer rings of Ag appear.

of Ag coverage, the mean particle size ($d$), the particle density ($n$) obtained from TEM, and the annealing temperature ($T_a$): (a) 0.6 ML, $d=1.6$ nm, $n=3.5\times10^{12}$ cm$^{-2}$, $T_a=670$ K, (b) 1.6 ML, $d=2.4$ nm, $n=2.8\times10^{12}$ cm$^{-2}$, $T_a=688$ K, (c) 3.2 ML, $d=3.1$ nm, $n=2.4\times10^{12}$ cm$^{-2}$, $T_a=760$ K, and (d) 4.8 ML, $d=3.7$ nm, $n=1.7\times10^{12}$ cm$^{-2}$, $T_a=782$ K. Ag nanocrystals formed with coverages of 0.6 and 1.6 ML show clear epitaxy of ⟨001⟩ orientation as indicated by the spotlike Ag reflections with [110] azimuth. In these two cases, surface reflections from the Si substrate are also observed as indicated by the arrows [Figs. 3(a) and 3(b)]. In contrast, for samples prepared at thicker Ag coverage, weak Ag diffraction rings still remain and additional Ag reflections with $[\bar{1}11]$ azimuth appear as indicated by the double-arrow head in Figs. 3(c) and 3(d). In these specimens, no surface reflections from the Si substrate are observed. The characteristic features of epitaxy can thus be summarized by the appearance of ⟨112⟩ orientation of Ag in addition to ⟨001⟩ orientation, as well as the remaining, weak Ag diffraction rings for the Ag coverage larger than 1.6 ML. Below that, epitaxy of Ag nanocrystals with ⟨001⟩ orientation dominates. This tendency is in contrast to the result for Ag/H-Si(111) system where the smaller Ag nanocrystals are less aligned than the bigger ones.[20]

The structure and morphology of Ag nanoparticles were characterized by TEM. HREM images and the corresponding SAED patterns for specimens with Ag coverage of 1.6 ML ($d=2.4$ nm) and 3.2 ML ($d=3.1$ nm) are shown in Figs. 4(a) and 4(b), respectively. Before the *ex situ* TEM observations, postdeposition annealing up to 680 and 748 K were performed for these specimens, respectively, together with *in situ* RHEED observations. Similar structural features are observed in both specimens as follows. The HREM images show the formation of squarelike Ag nanocrystals with sizes of 2–4 nm. Moiré fringes due to the lattice mismatch be-

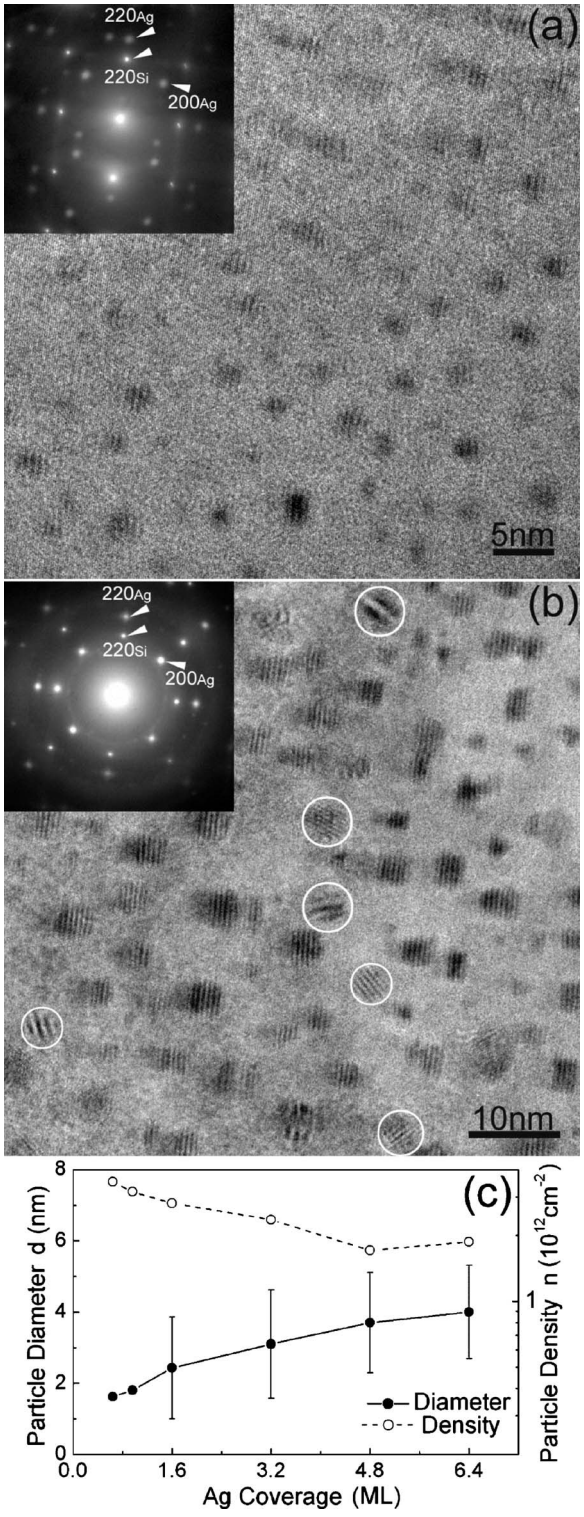


FIG. 4. HREM images and the corresponding SAED patterns. (a) 1.6 ML Ag coverage, after annealing at 680 K. The epitaxial orientation relationship can be seen in the SAED pattern. (b) 3.2 ML Ag coverage, after annealing at 748 K. Misoriented Ag nanocrystals are encircled in the image. (c) The dependence of the average particle size (solid circles) and particle density (open circles) as a function of Ag coverage. Error bars denote the standard deviation of the particle size distribution fitted by the log-normal distribution function.

tween Ag and Si are clearly seen in most of the Ag nanocrystals. Epitaxial growth of Ag nanocrystals is also confirmed by the directional moiré fringes in the HREM images. The SAED pattern shows the epitaxial relationship between the Ag nanocrystals and the Si(001) substrate with $(001)_{Ag}\|(001)_{Si}$ and $[110]_{Ag}\|[110]_{Si}$, which agrees with the RHEED observation as well as the previous study.[14] Besides the epitaxial diffraction spots, a weak $\{111\}_{Ag}$ ring is also observed in the SAED pattern for the Ag nanocrystals with 3.2 ML coverage. Misoriented Ag nanocrystals can be easily identified in HREM images by the direction of moiré fringes as those encircled in Fig. 4(b). Apparently, the dominant orientation of epitaxial Ag nanocrystals is $\langle 001\rangle$ rather than $\langle 112\rangle$ on the Si(001) surfaces. The average particle diameter and particle area density of Ag nanocrystals are summarized in Fig. 4(c) as a function of the Ag coverage. The size distribution histogram was fitted by a log-normal distribution function. This distribution is obtained when the logarithm of the particle size follows the Gaussian distribution, which is often observed in the self-assembly of metal nanoparticles by deposition.[21] The error bar indicates the standard deviation of the particle size distribution. Particle sizes were measured from the digital recorded TEM images and the total number of particles counted was more than 200 for each specimen. The particle size is defined here as the diameter of the circle having an area same as that of particles digitally measured from the TEM image. The observed smallest particle was about 1 nm in diameter. The average particle size increases from 1.6 to 4 nm in diameter as the deposited Ag coverage increases from 0.6 to 6.4 ML. It is worth mentioning that the size distribution of the Ag nanocrystals is rather narrow with the standard deviation between 1.3 to 1.5 nm. The particle area density gradually decreases as the average particle size increases. Overall, the particle density remains in the order of $10^{12}$ cm$^{-2}$. This is in agreement with the previous work.[14] The change in the particle size distribution histograms before and after annealing at 723 K is small.[14] This indicates that particle ripening is small during annealing and the effect of particle coalescence is also small to the epitaxial formation.

The above results show that the development of epitaxial nanocrystals is characterized by three characteristic, irreversible, temperatures: (1) The epitaxy formation temperature associated with the initial appearance of epitaxial nanocrystals in the RHEED patterns, (2) the temperature at which the intensity of Ag reflections start to decrease, and (3) the temperature at which the Ag reflections disappear as detected by RHEED. These three characteristic temperatures are summarized as a function of the average particle size in Figs. 5(a) (epitaxial formation temperature) and 5(b) (initial decrease and disappearance temperatures). The lines in Fig. 5(a) indicate the calculated melting temperatures for Ag nanoparticles as a function of the particle diameter using the following equation and different surface energies:[10,12]

$$T_M(d) - T_M = -\frac{4T_M}{\rho_S \Delta H_M d}\left[\gamma_S - \gamma_L\left(\frac{\rho_S}{\rho_L}\right)^{2/3}\right], \qquad (1)$$

where $T_M(d)$ is the melting temperature of a Ag nanoparticle with a diameter of $d$, $T_M$ is the melting temperature of bulk

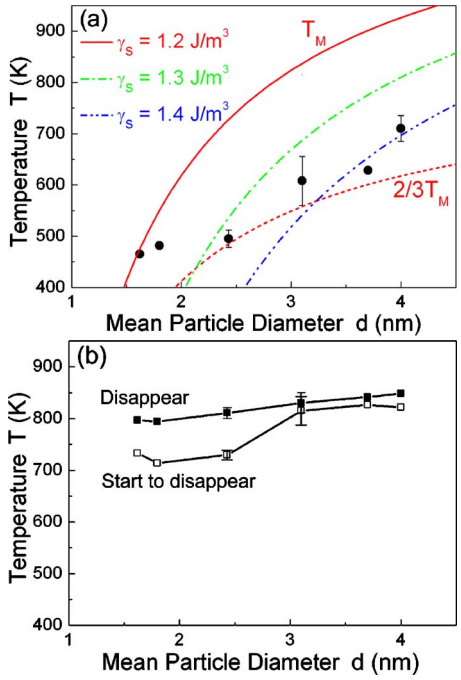


FIG. 5. (Color online) Particle size dependence of three characteristic, irreversible, temperatures for Ag nanoparticles as detected by RHEED observations. (a) The epitaxy formation temperature associated with the initial appearance of epitaxial nanocrystals (solid circles) and (b) the temperature at which the intensity of Ag reflections start to decrease (open squares) and the temperature at which the Ag reflections disappear (solid squares) as detected by RHEED, respectively. Solid and broken lines in (a) represent the theoretical size-dependent melting temperature for Ag and the 2/3 of the melting temperature calculated with $\gamma_S$=1.2 J/m$^2$, respectively.

Ag, $\Delta H_M$ is the latent heat of fusion of bulk Ag, $\rho$ is the mass density of the particle, $\gamma$ is the surface tension, and the subscripts $S$ and $L$ represent the solid and liquid phase of the particle at the melting point. Thermodynamic quantities of Ag used for drawing the solid line are as follows:[10,22] $T_M$ =1235 K, $\rho_S=9.82\times10^3$ kg/m$^3$, $\rho_L=9.33\times10^3$ kg/m$^3$, $\Delta H_M=1.11\times10^5$ J/kg, $\gamma_S$=1.2 J/m$^2$, and $\gamma_L$=0.895 J/m$^2$. The melting temperature expressed by Eq. (1) continuously decreases as the particle size reduces. The solid surface energy has a large effect on the melting temperatures. Figure 5(a) plots two additional melting temperature curves calculated with $\gamma_S$=1.3 J/m$^2$ and $\gamma_S$=1.4 J/m$^2$. The reported Ag surface energy ranges from 1.17 J/m$^2$ to 1.3 J/m$^2$ (Ref. 23 and 24). The lowest temperature for epitaxy is 465 K for 1.6-nm-sized Ag nanoparticles. The epitaxial formation temperature increases as the Ag coverage increases and reached 711 K for 4-nm-sized particles. For comparison, we also plotted the $\frac{2}{3}T_M(d)$ curves as shown in Fig. 5(a). The epitaxial formation temperatures are close to the $\frac{2}{3}T_M(d)$ curve calculated with $\gamma_S$=1.2 J/m$^2$ for particles larger than 2 nm. The epitaxial formation temperatures are close or above the melting temperatures if $\gamma_S$=1.4 J/m$^2$ is assumed. The two third of the melting temperature is regarded as a measure of an enough high temperature for atomic diffusion.[25] The epitaxial formation temperatures are 110–270 K lower than the temperatures when the disappearance of Ag was detected [open square in Fig. 5(b)]. It should be mentioned that the epitaxial formation temperature detected by RHEED is dominated by smaller Ag nanocrystals. The *ex situ* TEM observations show that the larger particles transform at higher temperatures than smaller particles. The small epitaxial particles contribute less to the RHEED intensity than large particles. Because of these two factors, the epitaxial formation temperature is primarily determined by medium sized particles and less affected by the experimental particle size distribution.

To consider the role of surface diffusion in the particle transformation, we consider the ratio of the surface atoms to the total atoms of an icosahedral particle. The ratio is 44.9% and 28.3% for 2-nm (561 atoms) and 4-nm-sized (2869 atoms) icosahedra, respectively.[3] The large population of the surface atoms facilitates fast migration and rearrangement of atoms, since the surface migration is usually much faster than bulk diffusion.[26,27] According to the computational study,[26] activation energy ($Q$) for surface migration of Ag adatom on Ag(100) is 0.48 eV with the frequency factor ($D_0$) of 1.2 or $3.9\times10^{-3}$ cm$^2$/s. The diffusion coefficient ($D$/m$^2$ s$^{-1}$) is given by

$$D = D_0 \exp(-Q/k_B T), \tag{2}$$

where $k_B$ and $T$ denote the Boltzmann constant and the temperature, respectively. Using the above reported parameters, the diffusion length ($\sqrt{D\tau}$; $\tau$: diffusion time) can be calculated to be 4 nm at 500 K for $10^{-5}$ s. This diffusion length is comparable to the size of the nanoparticle. On the contrary, the reported activation energy for bulk diffusion (self-diffusion) of Ag is about 1.76 eV with the frequency factor of 0.041 cm$^2$/s in the temperature range between 543 and 773 K[28]. These values lead to a short diffusion length of 0.03 nm even at 500 K for $10^2$ s. The above simple estimation indicates that surface migration of Ag atoms must play an important role in the size-dependent epitaxy.

As for the mechanism of epitaxial transformation of Ag nanoparticles, for particles smaller than 2 nm, there is a strong possibility of involving particle melting. The epitaxial formation temperatures are close to, or above, the theoretical size-dependent melting temperatures calculated using different surface energies. MD simulation shows that melting of free Ag nanoclusters initiates at the surface and proceeds toward the inside of the cluster as the temperature increases.[29] Such melting behavior can lead to high mobility of surface atoms especially for small nanoparticles. For nanoparticles larger than 2 nm, the uncertainty in the particle melting temperature makes it difficult to distinguish whether the particle does, or does not, melt for the structural transition.

Ag disappearance occurs at higher temperatures than the epitaxial formation temperature. There is a noticeable difference between the temperature at which the disappearance started and that when the Ag has disappeared. Thus the disappearance of Ag by evaporation and/or sublimation does not take place at a defined temperature. Furthermore, the difference becomes more prominent at lower Ag coverage as

shown in Fig. 5(b). The temperature differences between 64 and 81 K are observed for specimens with the Ag coverage of 0.6 to 1.6 ML, and 15–27 K for the samples with 3.2 to 6.4 ML Ag coverage. This difference is also seen in the temperature dependence of $(004)_{Ag}$ intensity shown in Figs. 1(i) and 2(i). Overall, disappearance of Ag completes in a narrow temperature range between 795 and 850 K for Ag nanocrystals of sizes between 1.6 and 4 nm. Apparently, the observed disappearance temperatures of Ag nanocrystals do not follow the melting temperature predicted by Eq. (1). One possible explanation of the observed size-independent evaporation and/or sublimation temperatures is size distribution of Ag nanocrystals. Assuming the kinematical theory of transmission electron diffraction, the intensity of diffracted beam ($I_g$) is expressed as follows:[30]

$$I_g = \left(\frac{\pi}{\xi_g}\right)^2 \frac{\sin^2 \pi s_g t}{(\pi s_g)^2} \rightarrow \left(\frac{\pi}{\xi_g}\right)^2 t^2 \quad (s_g \rightarrow 0), \tag{3}$$

where $\xi_g$, $s_g$, and $t$ denote the extinction distance of reflection $g$, excitation error of reflection $g$, and thickness, respectively. Note that presently observed Ag diffraction patterns are the so-called "transmission pattern" due to the island growth of Ag and the glancing angle diffraction geometry. In such a case, thickness $t$ in Eq. (3) corresponds to the lateral dimension of the Ag island. Thus Ag nanoparticles with large diameters contribute more to the diffracted beam intensity. Therefore, the observed melting and/or sublimation temperature for Ag is mainly determined by the large Ag nanocrystals. These nanocrystals have large curvatures, and low vapor pressure according to the kelvin equation.[16,31–34]

To check the disappearance of Ag from the Si surface, XPS spectra were measured for specimens with Ag thickness of 1.6 ML ($d$=2.4 nm) and 4.8 ML ($d$=3.7 nm). The obtained XPS spectra of Ag 3$d$ for both specimens are shown in Figs. 6(a) and 6(b), respectively. The energy scale was calibrated by using a Si 2$p$ peak position as a standard. In Fig. 6(a), solid and dotted lines denote the results for the as-deposited and the annealed specimens, respectively. Ag $3d_{3/2}$ and $3d_{5/2}$ peaks clearly disappeared after the annealing at 888 K. By contrast, the intensity of the Si 2$p$ peak was enhanced after the annealing (not shown), indicating the disappearance of Ag from the Si surface. The same tendency was observed in the other specimen with Ag coverage of 4.8 ML as shown in Fig. 6(b). Here, solid and dotted lines denote the results for the specimens after annealing at 782 and 873 K, respectively. A clear Ag 3$d$ peak can be seen after annealing at 782 K, while the peak disappeared for the sample annealed to 873 K. The maximum annealing temperature used is higher than the Ag reflection disappearance temperature indicated by RHEED. The XPS results also agree with TEM observations; no evidence of Ag nanoparticles was found in samples annealed above the temperatures where the Ag reflection disappeared.

To further examine the mechanism of Ag disappearance, we performed a detailed analysis of the RHEED intensity. Figure 7 shows a series of RHEED patterns recorded for Ag nanocrystals formed with the Ag coverage of 1.6 ML ($d$ =2.4 nm) and annealed. Figures 7(a)–7(d) are patterns observed at temperatures of 802, 818, and 888 K and the room temperature after cooling down, respectively. In Fig. 7(a), weak, but still spotlike, $(\bar{1}13)$ and $(004)_{Ag}$ reflections with $[110]_{Ag}$ azimuth are observed. This indicates the presence of epitaxial Ag nanocrystals at 802 K. At 818 K, the Ag reflections are no longer detectable in the RHEED pattern. The same is observed for the specimen heated up to 888 K. Figure 7(e) shows the temperature dependence of the integrated intensity of the $(\bar{1}13)_{Ag}$ reflections. The intensity profile was measured by taking a profile from the $(004)_{Si}$ reflection towards the $(\bar{1}13)_{Ag}$ reflection, and the integrated intensity was measured by fitting the profile using Lorentzian function. The intensity profile for the pattern observed at 818 K was used as the background intensity. Examples of intensity profiles are shown in Fig. 7(f). The intensity of the $(\bar{1}13)_{Ag}$ reflection started to decrease at 732 K, which continues until it disappears at 818 K. It must be emphasized that during annealing the epitaxial orientation of Ag nanocrystals was maintained. The Ag diffraction intensity decreases continuously until the Ag reflection disappeared. Thus we can assume that the amount of Ag decreases continuously on the Si(001) surface at the temperatures between 732 K and 818 K in this case. There are two possible mechanisms for the reduction of Ag: Melting and the subsequent evaporation or sublimation of Ag nanocrystals. The melting can start with the smaller Ag particles due to the size dependence of melting temperature. It is also possible that both mechanisms play a role in the disappearance of Ag nanocrystals. In study-

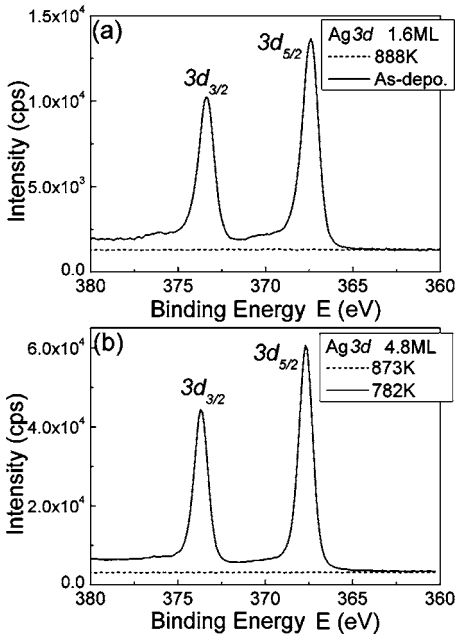


FIG. 6. XPS spectra for as-deposited and annealed Ag/H-Si(001) specimens: (a) Ag 3$d$ peaks of the 1.6-ML-coverage specimens. Solid and broken lines indicate the as-deposited and the annealed specimens, respectively. Annealing was carried out *in situ* up to 888 K. (b) Ag 3$d$ peaks of the Ag nanocrystals with 4.8 ML coverage after annealing at 782 K (solid line) and 873 K (broken line). Disappearance of Ag in both specimens is clearly seen.

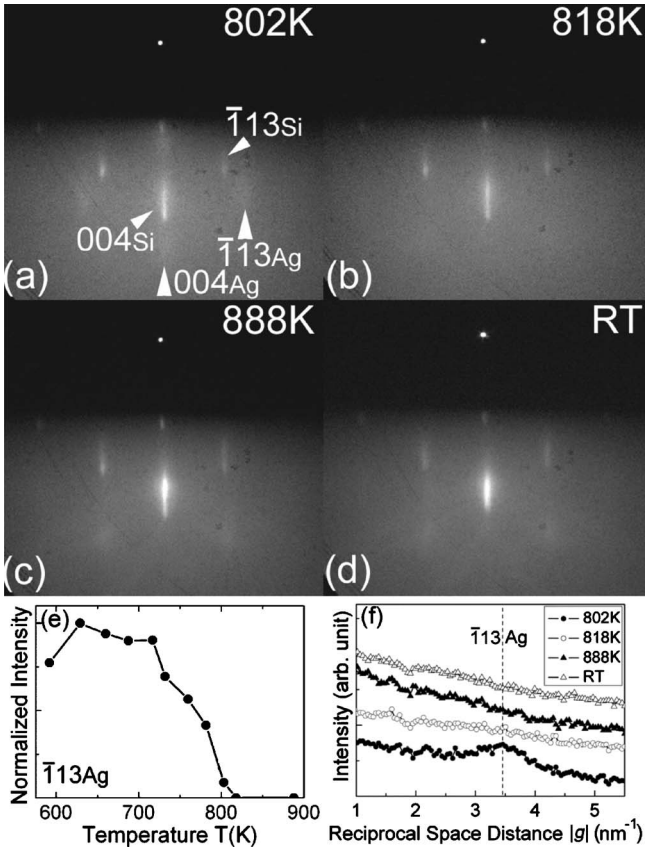


FIG. 7. Comparison of *in situ* RHEED patterns for Ag nanocrystals with 1.6 ML coverage: (a) 802 K, (b) 818 K, (c) 888 K, and (d) after cooling down to RT. Faint Ag reflections indexed as $(\bar{1}13)$ and (004) are seen at 802 K followed by the sudden disappearance at 818 K. Intensity profiles shown in the inset also show the disappearance of Ag. (e) Temperature dependence of the integrated intensity of $(\bar{1}13)_{Ag}$ reflection. (f) Intensity profiles on annealing measured from $(004)_{Si}$ toward $(\bar{1}13)_{Ag}$.

ing the evaporation of Au nanoparticles, Sambles reported that the radius of solid Au nanoparticles decreases continuously by sublimation and then the solid Au transforms into liquid and rapidly evaporates.[32] No halo diffraction rings of Ag could be detected in the course of annealing. Also no other diffraction spots, as well as rings from recrystallized Ag, were detected after cooling down. Diffuse diffraction rings are expected if part of nanocrystals melt and stay melt for a significant amount of time.[8] The lack of evidence for melting of Ag from our *in situ* RHEED observation can be a result of no melting or rapid evaporation of Ag particles after melting. Absence of melting is consistent with the previous reports. Continuous desorption of Ag from $Al_2O_3$ surface was measured by XPS,[35] where the intensity of Ag $3d_{5/2}$ peak disappeared at 900 K. In the study by Lee *et al.*[17], 9-nm-sized Ag nanoparticles were seen on the graphite substrate kept at 950 K and they disappeared by sublimation. In another study, vaporization of Ag atoms from the Si(111) surfaces was reported by an *in situ* RHEED observation at the temperatures above 973 K for a very thin Ag coverage of 0.1 nm.[36]

## IV. CONCLUSION

We have studied the structural transition from Ag MTPs to epitaxial fcc nanocrystals by means of *in situ* RHEED and *ex situ* TEM as a function of average particle sizes between 1.6 and 4 nm. Postdeposition annealing promoted the structural transition from MTP to epitaxial fcc nanocrystal. Full epitaxy of Ag nanoparticles was achieved when the particle average size is smaller than 2.4 nm. The orientation relationship is $(001)_{Ag}\|(001)_{Si}$, $[110]_{Ag}\|[110]_{Si}$, and this is identical to that observed by transmission electron diffraction in TEM. In contrast, weak Debye-Scherrer rings remained and additional Ag reflections appeared for particles larger than 3.1 nm. These additional reflections come from Ag nanocrystals with ⟨112⟩ texture with orientation relationship of $(1\bar{1}2)_{Ag}\|(001)_{Si}$. HREM image showed a small percentage of nanocrystals with this orientation. The dominant orientation of the Ag nanocrystals is ⟨001⟩ on the H-Si(001) surface after the structural transition. Clear particle size dependence was found in the epitaxial formation temperature. The lowest temperature was 465 K for 1.6-nm-sized Ag nanocrystals. The epitaxial formation temperature increases with the average particle size. The epitaxial formation temperatures can be approximately fitted by 2/3 of the calculated melting temperatures with $\gamma_S=1.2$ J/m$^2$ for particles larger than 2 nm. Disappearance of Ag nanoparticles was observed upon annealing at the temperature range between 795 and 850 K. In contrast to the clear size dependence of the epitaxial formation temperature, the disappearance of Ag took place within a relative narrow temperature range regardless of the particle size. No evidence of Ag melting could be detected by RHEED in the course of annealing. *Ex situ* TEM analysis confirmed the disappearance of Ag nanoparticles from the Si(001) surface after annealing to high temperatures. These results are consistent with sublimation of Ag from the Si(001) surfaces.

## ACKNOWLEDGMENTS

This work was supported by NSF DMR 0449790. The electron microscopy, Rutherford backscattering spectroscopy, and x-ray photoelectron spectroscopy analyses were carried out in the Center for Microanalysis of Materials, University of Illinois, which is partially supported by the US Department of Energy under Grant No. DEFG02-91-ER45439. The authors wish to thank R. Haasch for his help using XPS.

*Also at The Institute of Scientific and Industrial Research, Osaka University, Ibaraki, Osaka 567-0047, Japan.
[1] S. Ino, J. Phys. Soc. Jpn. **21**, 346 (1966).
[2] S. Ino, J. Phys. Soc. Jpn. **27**, 941 (1969).
[3] F. Baletto, R. Ferrando, A. Fortunelli, F. Montalenti, and C. Mottet, J. Chem. Phys. **116**, 3856 (2002).
[4] D. Reinhard, B. D. Hall, D. Ugarte, and R. Monot, Phys. Rev. B **55**, 7868 (1997).
[5] K. Koga, T. Ikeshoji, and K. I. Sugawara, Phys. Rev. Lett. **92**, 115507 (2004).
[6] B. W. van de Waal, Phys. Rev. Lett. **76**, 1083 (1996).
[7] P. Pawlow, Z. Phys. C **65**, 1 (1909); **65**, 545 (1909).
[8] M. Takagi, J. Phys. Soc. Jpn. **9**, 359 (1954).
[9] F. Baletto and R. Ferrando, Rev. Mod. Phys. **77**, 371 (2005).
[10] T. Castro, R. Reifenberger, E. Choi, and R. P. Andres, Phys. Rev. B **42**, 8548 (1990).
[11] I. Shyjumon, M. Gopinadhan, O. Ivanova, M. Quaas, H. Wulff, C. A. Helm, and R. Hippler, Eur. Phys. J. D **37**, 409 (2005).
[12] Ph. Buffat and J.-P. Borrel, Phys. Rev. A **13**, 2287 (1976).
[13] S. L. Lai, J. Y. Guo, V. Petrova, G. Ramanath, and L. H. Allen, Phys. Rev. Lett. **77**, 99 (1996).
[14] B. Q. Li and J. M. Zuo, Phys. Rev. B **72**, 085434 (2005).
[15] J. M. Zuo and B. Q. Li, Phys. Rev. Lett. **88**, 255502 (2002).
[16] J. R. Sambles, L. M. Skinner, and N. D. Lisgarten, Proc. R. Soc. London, Ser. A **318**, 507 (1970).
[17] J.-G. Lee, J. Lee, T. Tanaka, and H. Mori, Phys. Rev. Lett. **96**, 075504 (2006).
[18] M. Suemitsu, H. Nakazawa, and N. Miyamoto, Appl. Surf. Sci. **82/83**, 449 (1994).
[19] S. M. Gates, P. R. Kuntz, and C. M. Greenlief, Surf. Sci. **207**, 364 (1989).
[20] J. K. Bording, B. Q. Li, Y. F. Shi, and J. M. Zuo, Phys. Rev. Lett. **90**, 226104 (2003).
[21] C. G. Granqvist and R. A. Buhrman, J. Appl. Phys. **47**, 2200 (1976).
[22] *Binary Alloy Phase Diagrams*, 2nd ed., edited by T. B. Massalski, H. Okamoto, P. R. Subramanian, and L. Kacprzak (ASM International, Materials Park, OH, 1990), p. 92.
[23] L. Vitos, A. V. Ruban, and H. L. Skriver, Philos. Mag. B **78**, 487 (1998).
[24] L. Z. Mezey and J. Giber, Jpn. J. Appl. Phys., Part 1 **21**, 1569 (1982).
[25] P. Haasen, *Physical Metallurgy*, translated by J. Mordike (Cambridge University Press, Cambridge, UK, 1978), p. 288.
[26] C. L. Liu, J. M. Cohen, J. B. Adams, and A. F. Voter, Surf. Sci. **253**, 334 (1991).
[27] G. A. Bassett, in *Condensation and Evaporation of Solids*, edited by E. Rutner, P. Goldfinger, and J. P. Hirth (Gordon and Breach, New York, 1964), p. 599.
[28] N. Q. Lam, S. J. Rothman, H. Mehrer, and L. J. Nowicki, Phys. Status Solidi B **57**, 225 (1973).
[29] S. Zhao, S. Wang and H. Ye, J. Phys. Soc. Jpn. **70**, 2953 (2001).
[30] P. B. Hirsch, A. Howie, R. Nicholson, D. W. Pashley, and M. J. Whelan, *Electron Microscopy of Thin Crystals* (Krieger, Malabar, FL, 1977), pp. 156–160.
[31] R. Defay, I. Prigogine, and A. Bellemans, *Surface Tension and Adsorption*, translated by D. H. Everett (Longmans, Green, London, 1966), p. 243.
[32] J. R. Sambles, Proc. R. Soc. London, Ser. A **324**, 339 (1971).
[33] N. D. Lisgarten, J. R. Sambles, and L. M. Skinner, Contemp. Phys. **12**, 575 (1971).
[34] F. Piuz and J.-P. Borel, Phys. Status Solidi A **14**, 129 (1972).
[35] K. Luo, X. Lai, C.-W. Yi, K. A. Davis, K. K. Gath, and D. W. Goodman, J. Phys. Chem. B **109**, 4064 (2005).
[36] Y. Gotoh and S. Ino, Jpn. J. Appl. Phys. **17**, 2097 (1978).